ELSEVIER

Remote Sensing of Environment 81 (2002) 262–272

Remote Sensing of Environment

www.elsevier.com/locate/rse

# Coastal sea surface temperature variability from Landsat infrared data

Andrew Thomas*, Deirdre Byrne, Ryan Weatherbee

*School of Marine Sciences, University of Maine, Libby Hall 213, Orono, ME 04469-5741, USA*

Received 17 September 2001; received in revised form 24 October 2001; accepted 6 January 2002

**Abstract**

A time series of 23 Landsat Thematic Mapper (TM) band 6 thermal infrared images over the period 1986–1996 is used to quantify variability of sea surface temperature (SST) along the central coast of Maine, a morphologically complex region of bays, estuaries, and islands. An iterative regression scheme using coregistered, temporally coincident, daily composites of Advanced Very High Resolution Radiometer (AVHRR) Pathfinder SST data is used to scale the TM digital numbers in each scene to SST, approximating an atmospheric correction. This approach provides temporally concurrent match-ups, even for Landsat scenes more than 10 years old and over 1000 data points to most regressions. Analysis of the TM scenes by year–day delivers temporal resolution sufficient for insight into overall seasonal pattern and allows identification of recurring seasonal features within the study area. The dominant seasonal patterns is a cross-shelf SST gradient of coldest water nearshore in winter which reverses sign in summer and disappears in spring and fall. Differences in summer SST are evident between four adjacent bays, attributable to differences in residual circulation, freshwater input, and flushing. Recurrent frontal zones evident in summer are identified and compare well to available but noncoincident in situ hydrographic data. 

## 1. Introduction

Applications of satellite-measured sea surface temperature (SST) information in the coastal zone require temporal sampling frequencies sufficient to resolve ocean dynamics with spatial resolutions similar to those of terrestrial applications to resolve patterns within the bays, inlets, and estuaries of interest. At present, however, there is a distinct gap in the space/time/methodology sampling window afforded by the thermal infrared measurements made by meteorological satellites used in oceanographic applications (e.g., Advanced Very High Resolution Radiometer, AVHRR) and those available from satellite instruments optimized for terrestrial targets (e.g., LANDSAT Thematic Mapper, TM). The former typically employ spatial resolutions of 1–4 km and a wide (over 2000 km) swath width to deliver repeat coverage of a specific target location at temporal frequencies suitable for tracking dynamic weather and ocean processes — at least twice per day and usually more. Radiometers optimized for terrestrial applications deliver considerably higher spatial resolution, often 120 m or less, but at the expense of swath width. Given orbital constraints, revisit time for these sensors at a particular study site extends to weeks. Decorrelation time scales of processes in the coastal ocean, however, are hours to days meaning that a time series of such images conveys little information on dynamics. In addition, the operational requirement of meteorological/oceanographic instruments for accurate and calibrated SST information over the global ocean has demanded the use of sampling methodologies which enable a pixel-by-pixel atmospheric correction of the received radiance (Barton, 1995). Currently operational instruments optimized for terrestrial applications lack the internal capability for such an atmospheric correction, requiring additional independent information (e.g., Gibbons, Wukelic, Leighton, & Doyle, 1989; Schneider & Mauser, 1996; Vidal, Devaux-Ros, & Moran, 1997). When such information is available, the infrared fields derived from these instruments deliver high spatial resolution that can be exploited for coastal environmental work (e.g., Gibbons et al., 1989; Mustard, Carney, & Sen, 1999). Here, we present a coastal ocean environmental study in

* Corresponding author. Tel.: +1-207-581-4335; fax: +1-207-581-4388.

*E-mail address*: thomas@maine.edu (A. Thomas).

0034-4257/02/$ – see front matter 
PII: S0034-4257(02)00004-4

which the attributes of both a meteorological and a terrestrial remote sensing instrument are merged to quantify aspects of seasonal SST variability along a morphologically complex coastline.

The central coast of Maine, USA, is characterized by a highly irregular shoreline of islands, peninsulas, bays, and estuaries (Fig. 1). The region is dominated by Penobscot Bay, the second largest estuary on the US eastern seaboard, and Mount Desert Island. It is part of the Gulf of Maine, a temperate, highly biologically productive marginal sea of the northwest Atlantic. General circulation patterns within the Gulf of Maine are relatively well known (e.g., Brooks, 1985). Residual currents offshore in the study region are dominated by the southwestward flowing Eastern Maine Coastal Current (EMCC), a vertically well mixed and relatively cold current originating near the Canadian/American border (Pettigrew et al., 1998). Ecologically, the study region is of immediate interest as one of the most pristine coastal regions of the US, a historically productive coastal fishery and presently the most productive lobster habitat on the planet. It is now under increasing anthropogenic pressure from the competing interests of tourism, industry, aquaculture, the traditional fishing industry, and urban growth, yet the oceanography and hydrography of the bays, inlets, and very nearshore region remain poorly understood.

## 2. Background

In addition to its role in global climate and weather variability through surface heat flux, SST provides direct insight into the spatial and temporal variability of upper ocean currents, water mass boundaries, and mixing. SST fields measured by ships suffer from an unavoidable aliasing of the space–time dimensions because of the highly dynamic nature of ocean currents, a problem ameliorated by the synoptic measurements of satellites. The most readily available satellite SST data is from the AVHRR aboard the National Oceanic and Atmospheric Administration (NOAA) series of polar orbiting satellites. Under cloud-free conditions, these provide four to six images per day of a given target location with a maximum spatial resolution of 1.1 km at nadir, suitable for resolution of most temporal dynamics but poorly suited for spatial resolution within coastal bays.

Infrared energy received at the satellite is a sum of both that from the ocean surface as well as a vertical integral of that radiated/absorbed by the intervening atmosphere. Although relative patterns of surface temperature are often evident in images formed from total radiance, accurate estimates of the actual SST require removal of the intervening atmospheric signal, a so-called atmospheric correction. Since the incorporation of three thermal infrared channels into the AVHRR radiometer in 1981, centered at

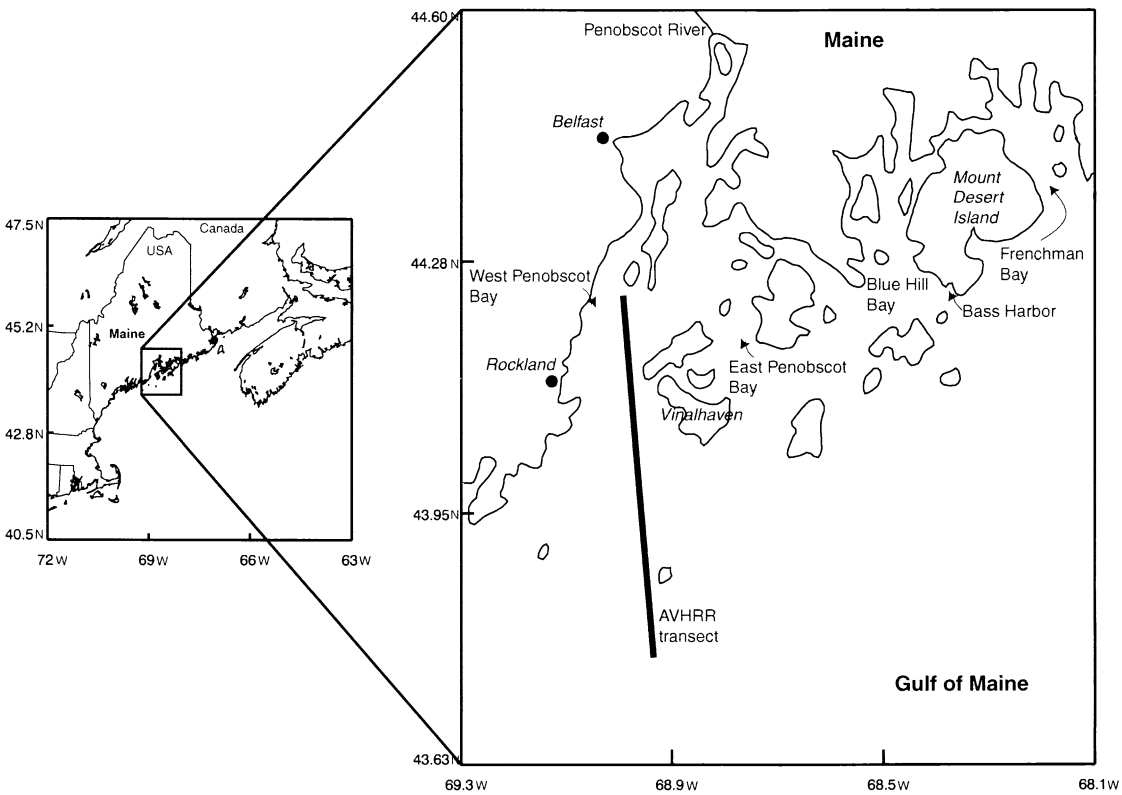


Fig. 1. The central coast of Maine study area showing larger islands, towns, and the four major coastal bays.

approximately 3.9, 10.9, and 11.9 μm, radiance retrievals from this instrument have been corrected to SST using a multichannel atmospheric correction based on a split window algorithm (McClain, Pichel, & Walton, 1985), the most recent of which is a nonlinear formulation (Walton, Pichel, Sapper, & May, 1998). The spectral window of Landsat TM Band 6 (10.4–12.5 μm) approximates AVHRR channels 4 and 5, but the single channel does not allow application of such an atmospheric correction to the radiance it measures.

## 3. Methods

An archive of 37 Landsat TM daytime images covering the central coast of Maine was acquired, spanning the time period from March 30, 1986 to June 26, 1996. All 37 were visually inspected for cloud and fog using both infrared and visible bands. Of these, 23 images proved sufficiently cloud-/fog-free over the coastal ocean to be useful. Chronologically, the temporal resolution of the dataset is extremely poor compared to timescales of importance in coastal dynamics. As shown by Mustard et al. (1999), however, arrangement of the images by year–day (Table 1) and taking a climatological approach to their analysis allows dominant and/or recurrent features within a canonical annual cycle to be characterized.

Band 6 from each TM image was extracted and georeferenced to a standard grid and projection covering the study region (Fig. 1) using ground control points. Pixels containing land were masked to a constant value. Although the spatial resolution of Band 6 is 120 m, the Level 9 Processed data delivered by the US Geological Survey are replicated to a 30-m pixel resolution using a cubic convolution to facilitate coregistration with the visible channels. All operations began with these 30 m pixels. NOAA AVHRR SST data coincident with the Landsat data were made available to us by the Graduate School of Oceanography, University of Rhode Island. SST in each image was calculated using the NASA/NOAA Pathfinder algorithm, an expansion beyond the nonlinear split window atmospheric correction based on regression of SSTs against a large, global match-up database of in situ surface measurements (Kilpatrick, Podesta, & Evans, 2001). The goal of the Pathfinder program is to produce a consistent time series of AVHRR SST measurements over interannual time scales. Kearns, Hanafin, Evans, Minnett, and Brown (2000) show that the mean difference between global Pathfinder SST products and SST recovered from a ship-mounted radiometer is $0.07 \pm 0.31$ °C for low and mid latitude data. Kilpatrick et al. (2001) state that the global Pathfinder SST product is within 0.02 °C of buoy SSTs within their database, with a standard deviation of 0.53 °C. Departures from these global statistics for local high resolution Pathfinder product used here likely exist, however, the use of absolute SST values in this study is restricted to seasonal differences, significantly larger in range (> 10 °C) than any of the cited statistics. Other analyses focus on relative temperature patterns within scenes. Pathfinder AVHRR SST images were georeferenced to a standard grid

Table 1
Dates of LANDSAT TM and AVHRR Pathfinder image pairs

| Month | Day | Year | Gain[a] | Intercept[b] | Iterations | $N$[c] | $r^2$ |
|---|---|---|---|---|---|---|---|
| February | 03 (034) | 1995 | 1.2 | 85.9 | 6 | 2388 | .78 |
| February | 18 (039) | 1989 | 1.6 | 84.0 | 5 | 2580 | .89 |
| March | 09 (068) | 1990 | 1.6 | 85.5 | 4 | 3861 | .91 |
| March | 30 (089) | 1986 | 1.4 | 87.7 | 3 | 3100 | .72 |
| April | 08 (098) | 1995 | 0.9 | 87.9 | 4 | 2751 | .83 |
| April | 15 (105) | 1986 | 0.9 | 89.0 | 5 | 2533 | .67 |
| May | 28 (148) | 1990 | 0.8 | 93.2 | 6 | 2095 | .64 |
| June | 26 (177) | 1989 | 0.7 | 101.9 | 6 | 491 | .60 |
| June | 27 (178) | 1995 | 1.8 | 85.0 | 3 | 3250 | .83 |
| June | 29 (180) | 1996 | 0.8 | 101.1 | 5 | 1503 | .70 |
| July | 18 (199) | 1991 | 0.7 | 102.4 | 6 | 1738 | .70 |
| August | 03 (215) | 1991 | 0.9 | 102.1 | 6 | 883 | .57 |
| August | 05 (217) | 1986 | 1.3 | 92.4 | 5 | 2263 | .76 |
| August | 14 (226) | 1995 | 1.1 | 98.1 | 4 | 603 | .52 |
| September | 06 (249) | 1989 | 1.4 | 83.3 | 4 | 2515 | .71 |
| September | 12 (255) | 1994 | 1.5 | 87.4 | 6 | 1025 | .72 |
| September | 25 (268) | 1993 | 1.4 | 90.2 | 3 | 3580 | .75 |
| September | 27 (271) | 1988 | 1.0 | 92.9 | 5 | 2102 | .69 |
| September | 30 (273) | 1989 | 1.1 | 93.0 | 4 | 3107 | .72 |
| October | 03 (276) | 1990 | 1.4 | 89.5 | 4 | 3152 | .76 |
| November | 20 (324) | 1990 | 0.4 | 95.9 | 6 | 514 | .36 |
| December | 19 (353) | 1989 | 2.0 | 84.9 | 4 | 3604 | .88 |
| December | 27 (362) | 1992 | 2.2 | 82.1 | 3 | 3675 | .92 |

[a] DN/°C Pathfinder SST.
[b] DN.
[c] Number of final pixel match-ups after all iterations.

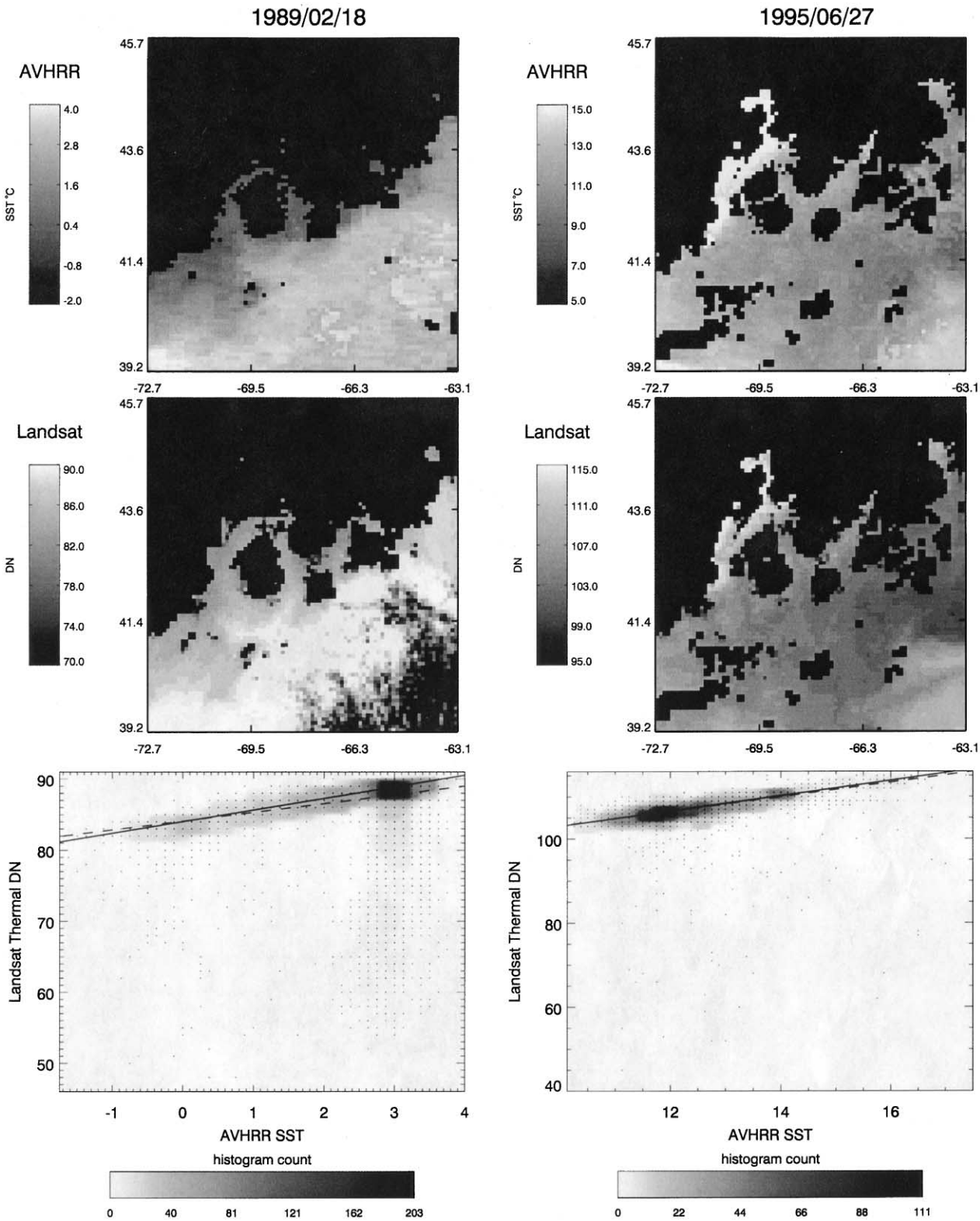


Fig. 2. Two examples of Pathfinder AVHRR daily composite and Landsat TM image pairs illustrating the pixels used in the location match-ups, the effects of AVHRR cloud-masking and land/cloud dilation, and the effects of Landsat spatial filtering to approximate AVHRR spatial resolution. Below each pair is the resulting linear regression of AVHRR Pathfinder SST against Landsat TM Band 6 DN showing the initial regression (dashed line) and the final regression (solid line) made after iteratively removing values more than one standard deviation from each successive regression and redoing the calculation. Coefficients and statistics for these two regressions are given in Table 1.

and projection at a spatial resolution of 1.25 km, land pixels were masked to a single value, as were pixels contaminated by cloud and/or fog (Cayula & Cornillon, 1996; Ullman & Cornillon, 1999). This AVHRR SST dataset consists of 5–6 scenes per day. For each Landsat image, all AVHRR SST scenes from the same date were composited to form a single SST image representative of mean conditions over that day. This 23-image AVHRR series was then visually inspected. Regions in two of the scenes that appeared to have poorly masked clouds were manually flagged. Formation of daily composites from the AVHRR data proved preferable the single selecting AVHRR scene closest in time to the Landsat overpass, as even this time separation meant that clouds moving through the study area inevitably reduced the number of usable pixels in the AVHRR scene. Significantly more match-ups became available using daily AVHRR composites. Regressing the TM data to a daily mean of five to six AVHRR scenes from both day and night also reduces the effect of diurnal SST skin temperature variability that might arise from differences in the orbit time of LANDSAT and any single AVHRR overpass. Some effects caused by the interaction of diurnal SST variability and image times, however, undoubtedly remain and contribute to variability observed in the regression statistics.

Landsat DN values were mapped to SST by regression against temporally and spatially coincident AVHRR SST values. This approach to atmospheric correction assumes a spatially homogenous atmosphere. While contributing to overall errors, this is a reasonable assumption for the relatively small geographic region considered here (approximately 100 km in latitude and longitude). To maximize the quality of the SST values going into the regression a morphological dilation operation was applied to each AVHRR composite, dilating the land-mask and cloud mask by one pixel (Fig. 2). This significantly reduced the number of pixels containing partial land or poorly flagged cloud entering the regression. In the ocean area remaining, the geographic center of each AVHRR pixel was determined and the SST value at each was extracted. Under cloud-free conditions, 4561 of these fell within the study region covered by the Landsat TM imagery. To account for the differing spatial resolution of the two data sets, Landsat TM images were low-pass filtered in the spatial domain using a $41 \times 41$-pixel kernel. This averaged the DN values of the many Landsat pixels that fall within one AVHRR pixel, approximating an independent DN estimate at each of the AVHRR pixel centers (Fig. 2). DN values at the 4561 geographic locations were then extracted and retained. Protocols exist to transform Band 6 DN values to radiance and then to uncorrected blackbody temperature values (Gibbons et al., 1989). These transformations are linear, however, and here we use Band 6 DN values as delivered for input to our regressions. For each AVHRR/TM image pair, a linear regression was computed on those match-up locations that had valid (cloud-free) Pathfinder SST measurements (Fig. 2 and $N$ in Table 1). Final coefficients for the regressions were determined in an iterative manner to reduce the effect of pixels contaminated by cloud and fog that were inevitably present in the TM DN values (Elvidge, Yuan, Weerackoon, & Lunetta, 1995). Match-up values more than one standard deviation away from the initial regression were discarded and the regression was then recalculated using the subset values. This process was repeated up to a maximum of six iterations until the gain and bias estimates stabilized (Fig. 2). Regression coefficients specific to each date (Table 1) were then used to scale DN values across the whole TM scene to SST (°C).

## 4. Results and discussion

### 4.1. Regressions

Gains and intercepts for the 23 regressions (Table 1) are relatively stable although one slope appears low (November 1990). The mean gain is 1.2 DN/°C with 17 of the 23 scenes falling within the range 0.7–1.5 DN/°C. Gibbons et al. (1989) show the thermal resolution of corrected TM data to be $\sim$0.6 °C which compares well with our values of 0.8 °C. The mean intercept is 91.1 DN with 18 of the 23 values in the range 82.1–95.9 DN. Variability introduced from a

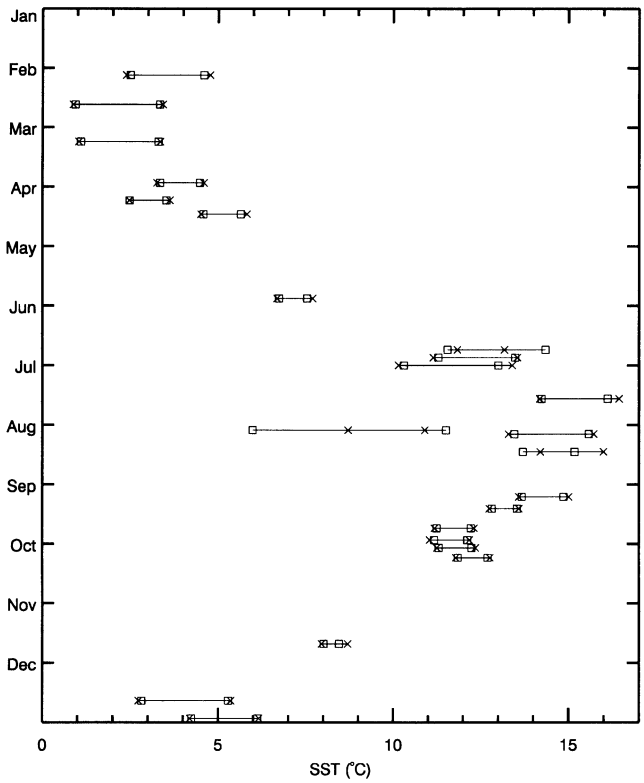


Fig. 3. The times series of SST in coincident Pathfinder AVHRR SST and calibrated Landsat TM SST pixel match-ups (see Fig. 2) for each of the 23 study images. These arranged in order of year–day to illustrate their depiction of the climatological seasonal cycle. Horizontal bars show ±1 standard deviation of SST (□ for AVHRR, × for Landsat).

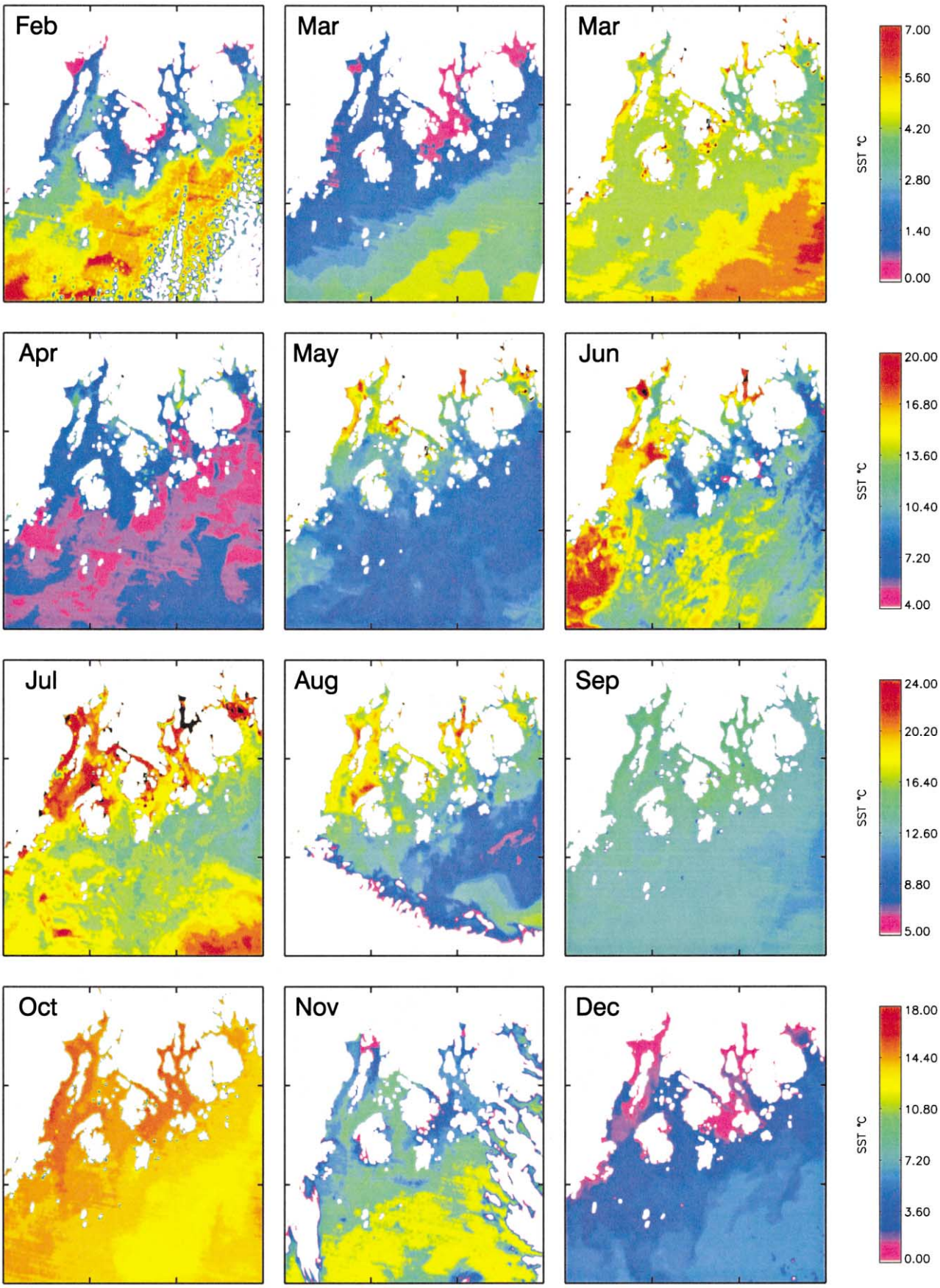
Feb
Mar
Mar
SST °C
7.00
5.60
4.20
2.80
1.40
0.00
Apr
May
Jun
SST °C
20.00
16.80
13.60
10.40
7.20
4.00
Jul
Aug
Sep
SST °C
24.00
20.20
16.40
12.60
8.80
5.00
Oct
Nov
Dec
SST °C
18.00
14.40
10.80
7.20
3.60
0.00

number of sources contributes to the observed instability of both gain and intercept within these ranges. The most obvious are surface skin effects, caused primarily by variability in wind speed, air–sea temperature differences and humidity, and variability in the atmospheric profile through which the surface-leaving radiance must propagate. These affect both the AVHRR and TM data and likely vary significantly between the temporally separated images. TM data also contain coherent noise (e.g., Zhang, Carder, Lee, Muller-Karger, & Goldgof, 1999) which leads to systematic pattern in the imagery. Errors introduced by these patterns are ameliorated by the spatial filtering, but remain in the data. Other factors also contribute to the variability in gain and intercept between scene pairs, including nonhomogeneity of the atmosphere (including unresolved fog and cloud) over the scene, differences in tidal phase and stratification and temporal bias remaining in the daily AVHRR composite–TM comparison created by any missing data in the AVHRR series over a day.

One advantage of using concurrent AVHRR data as opposed to in situ measurements for regression is evident in the large number of temporally concurrent pixel match-ups that are available (Table 1). Statistical significance of the correlation coefficients is a function of the degrees of freedom, which is dependent upon the number of independent observations. Independence of surface SST measurements is a function of local spatial decorrelation scales of SST which reduce the effective degrees of freedom from the N shown in Table 1. We calculated spatial autocorrelation functions from example Pathfinder daily composites and estimate decorrelation scales (from the first zero crossing) in this coastal area to be of order 20 km. This suggests that even for N/400, the majority of regressions in Table 1 are significant at the 95% level. We also suspect that the daily composites overestimate actual decorrelation scales. As expected, the variability present in the regression coefficients due to changing atmospheric conditions means that an overall mean gain and intercept cannot be used to scale Landsat DN to SST. In most cases, the resulting variability in SST in the Landsat data is similar to that of the AVHRR data (Fig. 3). The most obvious differences (e.g., August 1991) are due to unmasked cloud/fog for in the Landsat scenes. More subtle differences are due to differences in the spatial resolution of the two sensors and the temporal difference represented by the images. The overall annual cycle of SST averaged over the entire study region, however, is clearly evident in both data sets (Fig. 3) and is presented in Fig. 4 as a time series of 12 individual day scenes chosen from the 23 available scenes. The one clear outlier from the cycle (August 3, 1991), is most likely biased by both unmasked cloud contamination in the Landsat data as well as the fact that clouds obscure the warmest ocean regions of the scene.

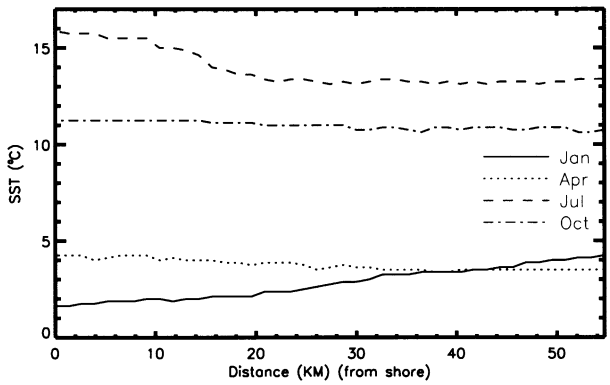


Fig. 5. Four cross-shelf SST profiles from western Penobscot Bay (Fig. 1) in January, April, July, and October, sampled from climatological (1985–1997) monthly composites of AVHRR Pathfinder images. These illustrate the change in gradient sign from winter (January, colder within the bays and warmer offshore) to summer (July, warmer within bays, colder offshore), separated by relatively isothermal conditions in spring and fall (April and October).

Use of AVHRR SST data avoids the need for a detailed in situ data set coincident with each Landsat overpass. Such data are often not available, prohibiting the correction of some Landsat scenes especially for retrospective work, or match-up data are separated temporally, reducing their value. In addition, in situ data collection is often logistically difficult and expensive. While in situ data can provide adequate match-ups, the use of AVHRR data readily yields many hundreds of data points as input to a regression. Our approach assumes that regression coefficients developed from AVHRR pixels in the immediate offshore region are applicable to TM pixels within small bays unresolved by the AVHRR. This assumption may be violated in some locations/times when strong and small spatial scale cross-shore differences in atmospheric conditions occur.

### 4.2. Surface temperature patterns

The time series of Landsat SST images resulting from the empirical atmospheric correction effectively illustrate fine scale SST spatial variability within the study area. Temporal separation between images, however, restricts interpretation to those features that are recurrent either within or between seasons over the multiple years used in the study. A time series of 12 TM SST images chosen to illustrate SST patterns in each calendar month is given in Fig. 4 (no images for January are available).

Fig. 4. A time series of 12 calibrated Landsat TM Band 6 images illustrating SST patterns within the central coast of Maine study area by calendar month over an annual cycle. Image dates are February 3, 1995; March 9, 1990; March 30, 1986; April 15, 1986; May 28, 1990; June 29, 1996; July 18, 1991; August 3, 1991; September 25, 1993; October 3, 1990; November 20, 1990; and December 19, 1989. Note the change in color scale used to allow improved visualization of surface thermal patterns in each season.

The dominant signal evident in the Landsat SST time series is a large-scale cross-shelf thermal gradient that changes sign over the seasonal cycle. The temperate latitude and eastern continental location of the study site impose a strong seasonal cycle of heat flux on the upper water column. In deeper offshore waters influenced by the vertically mixed water of the EMCC, the effect of this heat flux seasonal cycle on SST is diminished. Within relatively sheltered inlets and bays, however, the data show that the seasonal cycle in SST is amplified. Strong winter cooling from the surrounding landmass and summer surface heating of inshore regions of reduced flushing and connection with the open Gulf of Maine result in extremes of seasonal amplitude. Early in the year (February–March, Fig. 4), warmest temperatures are offshore in the Gulf of Maine within EMCC (4–6 °C) and coldest SST is present within the bays (<2.0 °C). During spring (April), vertical mixing and greater water depths offshore allow the surface water within the bays to warm more quickly and this gradient is reduced. Cross-shelf SST patterns become more isothermal.

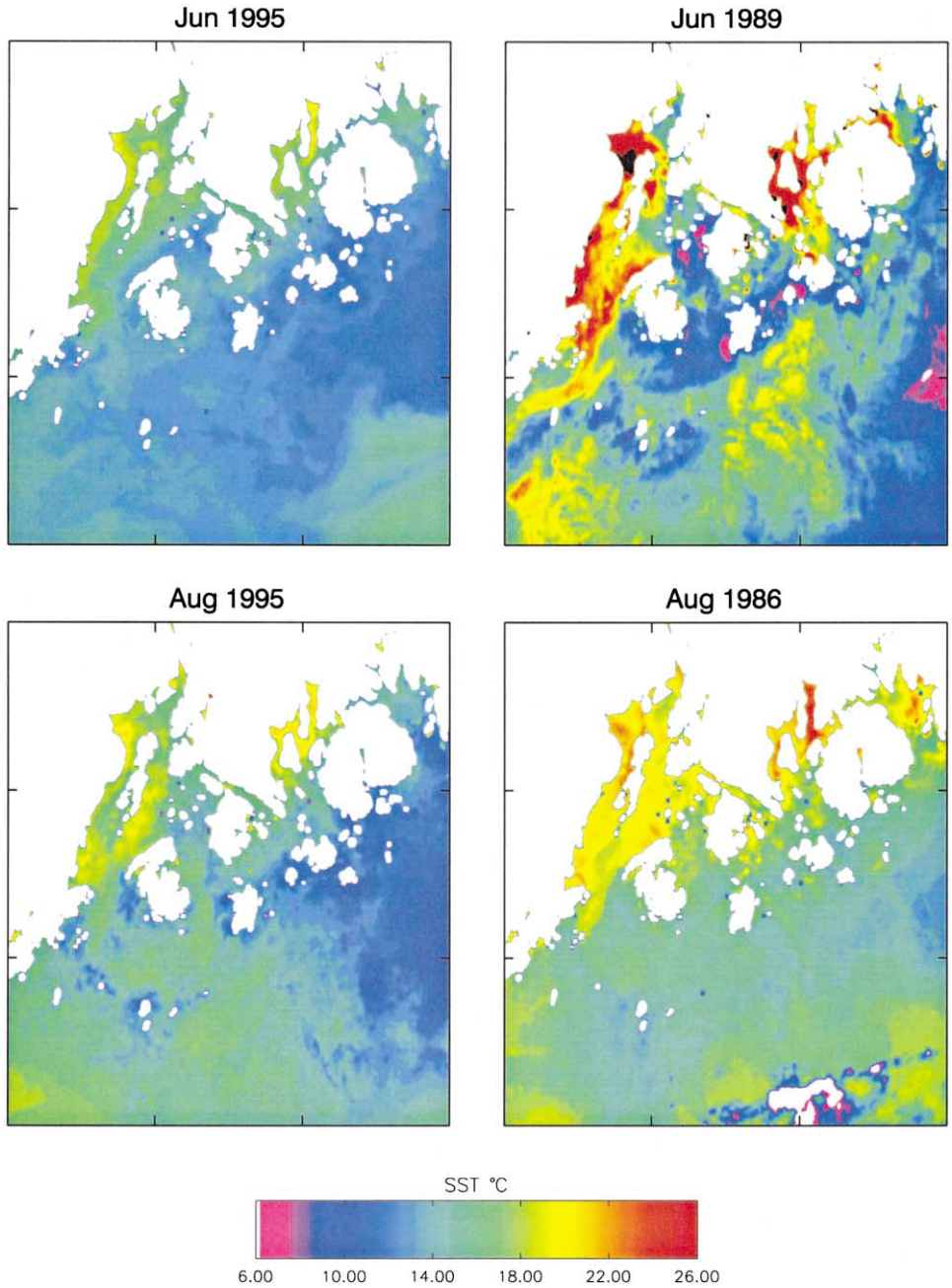


Fig. 6. Four calibrated Landsat TM Band 6 SST scenes from the summer period of maximum surface thermal heterogeneity showing consistent temperature differences between the four major bays within the study area, as well as persistent frontal features near the entrances to west Penobscot Bay and Blue Hill Bay. Image dates are (a) June 27, 1995; (b) June 26, 1989; (c) August 14, 1995; and (d) August 5, 1986.

By May (Fig. 4), heating within the bays, coupled with continued vertical mixing of offshore water, has reversed the gradient and offshore waters are cooler than those inshore. This pattern strengthens through the summer (June, July, August) and then weakens in fall (September, October). The only available November image (1990) shows warmest temperatures offshore again.

The 120-m resolution of the Landsat SST scenes shows details of this large-scale thermal gradient into each of the major bays and channels within the study area that AVHRR scenes cannot. Direct sampling of this gradient from the AVHRR data can be made, however, within the West Penobscot Bay channel, which is wide enough to allow subsampling from the 1.25 km resolution data. In addition, the daily AVHRR data provide enough samples to create statistically robust monthly means, allowing a temporal quantification of cross-shelf seasonal cycles. Climatological monthly composites of the AVHRR pathfinder data were formed from 13 years of available data (1985–1997) and a cross-shelf transect down the center of West Penobscot Bay Channel (see Fig. 1) was subsampled from each of the 12 resulting scenes. SST profiles (Fig. 5) for four of these months demonstrate the seasonally varying sign and strength of the cross-shelf SST gradient, showing it to be a consistent feature of the SST climatology of the region.

A second pattern of SST variability evident in the image sequence is a consistent difference in the surface thermal regime during nonwinter months between the four major bays within the study area (Fig. 1). During winter, isothermal SST conditions exist across the entire inshore domain, the result of strong, large-scale cooling over the region (Fig. 4). Once increased heating and reduced wind mixing allows vertical stratification to begin in spring, however, differences in circulation, vertical mixing, and connection to offshore colder water create differences in the surface thermal regime between east Penobscot Bay, west Penobscot Bay, Blue Hill Bay, and Frenchman Bay which become evident in the Landsat SST data. West Penobscot Bay and Blue Hill Bay are consistently warmer than east Penobscot Bay and Frenchman Bay in each of the available Landsat scenes over the period June to September (Table 1). Four of these TM SST daily images are shown in Fig. 6. In Penobscot Bay, the SST difference between the two main channels is likely due to interaction between residual circulation, estuarine outflow of Penobscot River water that enters at the head of the bay and vertical mixing induced by tidal flow over shallow bathymetry. Consistent with oceanographic theory in which Coriolis turns flow to the right in the northern hemisphere, field data (unpublished) indicate that the majority of freshwater entering the head of Penobscot Bay flows down the west (right) side and exits the bay through the west channel. Increased vertical stability within this buoyant plume would allow surface waters to heat more rapidly than surrounding water and contribute to warmer temperatures on the western side. Field data also show (N. Pettigrew, University of Maine, personal communication) residual flow of surface water in East Penobscot Bay is to the south, out of the bay. The relatively cold surface temperatures here are likely a result of strong tidal mixing which occurs in the complex and relatively shallow channel system that separates the east Bay from the west Bay. Relatively well mixed and colder SST water is then advected out along the east channel into the Gulf of Maine. Comprehensive field data do not exist for the Blue Hill Bay and Frenchman Bay areas and the Landsat data shown here provide the first synoptic comparison of these bays. Freshwater input into both is significantly less than that of the Penobscot River but is larger in Blue Hill Bay. The consistently warmer surface temperatures within Blue Hill Bay most likely reflect increased vertical stratification due to this freshwater and the presence of longer channels (distance from the open Gulf of Maine) and many islands which lead to increased isolation and reduced flushing. The images show that Frenchman Bay has a shorter, more direct connection to colder water in the Gulf of Maine.

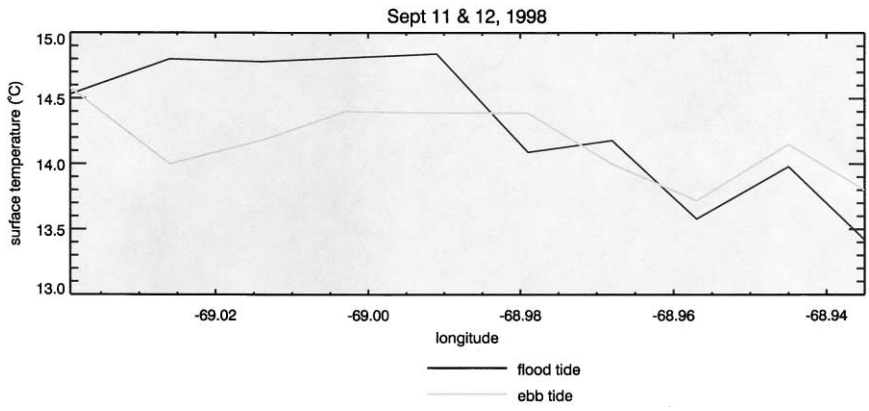


Fig. 7. Ship-measured surface temperature from early September 1998 during two phases of the tide across the mouth of west Penobscot Bay from Rockland to Vinalhaven showing the cross-channel frontal zone separating warmer surface water on the west (mainland) side from colder surface water on the east (Vinalhaven) side.

The spatial resolution of the Landsat scenes show a diversity of small scale thermal features within the study area (Fig. 6). The temporal separation between images however, means that only the most persistent features can be interpreted with any confidence. In each summer image, a strong frontal zone is evident in the western Penobscot Bay entrance channel between the mainland and Vinalhaven. This frontal zone is oriented approximately along the channel and separates colder SSTs on the Vinalhaven side from warmer SSTs on the mainland side. This surface thermal feature is consistent with in situ hydrographic data which show that warmer surface water which exits Penobscot Bay through the western channel does so on the mainland side with colder SSTs present on the Vinalhaven side (Fig. 7). The pattern is also consistent with anecdotal stories from the ferry that runs between Rockland and Vinalhaven of clear skies in Rockland and persistent spring/summer fog on the Vinalhaven side of the channel. A second persistent feature is the presence of a frontal zone within the island archipelago at the entrance to Blue Hill Bay. This frontal zone varies strongly in precise position and orientation between images but consistently leaves the seaward tip of Mount Desert Island (Bass Harbor area) within the cold SST regime of the open Gulf of Maine imposing a significantly different marine regime on this area compared to surrounding coastal regions. Other strong frontal zones are evident within individual images, likely a result of interactions between tidal mixing/advection and residual circulation. Interpretation of these more ephemeral features, however, requires either in situ or satellite data at time/space resolutions unavailable to us at present.

## 5. Summary and conclusions

A time series of 23 Landsat TM band 6 images spanning the period 1986–1996 was atmospherically corrected by regression with concurrent AVHRR Pathfinder SST data to provide 120 m resolution SST images of a morphologically complex temperate coastal region. Atmospheric variability between TM scenes requires that temporally coincident ground truth data be used for such a regression. The obvious difficulty in meeting this requirement with a field program highlights the utility of using readily available AVHRR SST data as ground truth. The approach assumes a spatially homogeneous atmosphere over the study region. In addition to atmospheric variability, factors such as seasonal and weather related differences in surface skin temperatures and tidal phase all contribute to the observed variability of the regression coefficients.

While delivering spatial resolution sufficient to resolve SST variability within the small bays and channels of the study area, the 16 day repeat cycle of Landsat coupled with cloud cover prohibit resolution of temporal variability on scales shorter than seasonal. Arranged by year–day, the TM scenes were examined for SST patterns indicative of seasonal variability and recurrent/persistent features. The dominant SST feature is a seasonally varying cross-shelf gradient, with warmest water inshore and colder SST offshore during summer, the inverse of this in winter and spatially homogeneous SST in spring and fall. This pattern was confirmed by comparison to climatological monthly AVHRR composites, subsampled within the largest cross-shelf channel of the study area. Smaller scale spatial SST variability within the study region was maximum during summer and minimal during winter due to large scale cooling. The four major bays within the study area exhibit differing mean SSTs during summer months. Both East Penobscot Bay and Frenchman Bay were consistently cooler than West Penobscot Bay and Blue Hill Bay in the TM images, most likely due to interactions with residual circulation, tidal mixing and freshwater influence. Two frontal features at the entrances to major channels were also recurrent features within the summer imagery, one of which could be confirmed with field data.

An improved ability to quantify surface thermal variability in coastal regions at the time and space scales necessary to resolve relevant dynamics awaits the development and launch of a new earth observation mission. This mission will require radiometer characteristics capable of local atmospheric correction, at least the repeat/revisit cycle afforded by the NOAA satellite series coupled with a spatial resolution of order 100 m. Until such data are available, however, merging the optimal characteristics of AVHRR and Landsat offers one approach to bridging the current temporal/spatial gap in capabilities.

## Acknowledgments

Funding for this study was provided by NOAA NESDIS through the Penobscot Bay Research Collaborative, by NASA Grant NAG5-6558, and by the Maine Science and Technology Foundation. We thank the Island Institute for their efforts in organizing and managing the Collaborative, our fellow Collaborative investigators for many insightful discussions on the dynamics of the study region and Peter Cornillon, University of Rhode Island, for access to the extensive AVHRR Pathfinder archive. Neal Pettigrew provided hydrographic data from western Penobscot Bay.

## References

Barton, I. J. (1995). Satellite-derived sea surface temperatures: current status. *Journal of Geophysical Research*, *100*, 8777–8790.

Brooks, D. A. (1985). Vernal circulation in the Gulf of Maine. *Journal of Geophysical Research*, *90*, 4687–4705.

Cayula, J. F., & Cornillon, P. (1996). Cloud detection from a sequence of SST images. *Remote Sensing of the Environment*, *55*, 80–88.

Elvidge, C. D., Yuan, D., Weerackoon, R. D., & Lunetta, R. S. (1995). Relative radiometric normalization of Landsat Multispectral Scanner

(MSS) data using an automatic scattergram-controlled regression. *Photogrammetric Engineering and Remote Sensing*, *61*, 1255–1260.

Gibbons, D. E., Wukelic, G. E., Leighton, J. P., & Doyle, M. J. (1989). Application of Landsat Thematic Mapper data for coastal thermal plume analysis at Diablo Canyon. *Photogrammetric Engineering and Remote Sensing*, *55*, 903–909.

Kearns, E. J., Hanafin, J. A., Evans, R. H., Minnett, P., & Brown, O. T. (2000). An independent assessment of Pathfinder AVHRR SST using the Marine Atmosphere Emitted Radiance Interferometer (MAERI). *Bulletin of the American Meteorological Society*, *81*, 1525–1536.

Kilpatrick, K. A., Podesta, G. P., & Evans, R. (2001). Overview of the NOAA/NASA AVHRR Pathfinder algorithm for sea surface temperature and associated matchup database. *Journal of Geophysical Research*, *106*, 9179–9198.

McClain, E. P., Pichel, W. P., & Walton, C. C. (1985). Comparative performance of AVHRR-based multichannel sea surface temperatures. *Journal of Geophysical Research*, *90*, 11587–11601.

Mustard, J. F., Carney, M. A., & Sen, A. (1999). The use of satellite data to quantify thermal effluent impacts. *Estuarine, Coastal and Shelf Science*, *49*, 509–524.

Pettigrew, N. R., Townsend, D. W., Xue, H., Wallinga, J. P., Brickley, P. J., & Hetland, R. D. (1998). Observations of the Eastern Maine Coastal Current and its offshore extension. *Journal of Geophysical Research*, *103*, 30623–30640.

Schneider, K., & Mauser, W. (1996). Processing and accuracy of Landsat Thematic Mapper data for lake surface temperature measurement. *International Journal of Remote Sensing*, *17*, 2027–2041.

Ullman, D., & Cornillon, P. (1999). Satellite-derived sea surface temperature fronts on the continental shelf off the northeastern US coast. *Journal of Geophysical Research*, *104*, 23459–23478.

Vidal, A., Devaux-Ros, C., & Moran, S. M. (1997). Atmospheric correction of Landsat TM thermal band using surface energy balance. *Remote Sensing Review*, *15*, 23–33.

Walton, C. C., Pichel, W. G., Sapper, F. J., & May, D. A. (1998). The development and operational application of nonlinear algorithms for the measurement of sea surface temperatures with NOAA polar-orbiting environmental satellites. *Journal of Geophysical Research*, *103*, 27999–28012.

Zhang, M., Carder, K., Lee, Z., Muller-Karger, F. E., & Goldgof, D. B. (1999). Noise reduction and atmospheric correction for coastal applications of Landsat TM imagery. *Remote Sensing of the Environment*, *70*, 167–180.